Journal of the European Ceramic Society 36 (2016) 741–748

Contents lists available at www.sciencedirect.com

Journal of the European Ceramic Society

journal homepage: www.elsevier.com/locate/jeurceramsoc

Finite-element modeling of the electro-thermal contacts in the spark plasma sintering process

C. Manière [a,b,c], A. Pavia [a,b], L. Durand [c], G. Chevallier [a,b], K. Afanga [a,b], C. Estournès [a,b,*]

[a] Université de Toulouse, Institut Carnot Cirimat, UPS CNRS, Université Paul-Sabatier, 118 route de Narbonne, 31062 Toulouse Cedex 9, France
[b] CNRS, Institut Carnot Cirimat, 118 route de Narbonne, 31602 Toulouse Cedex 9, France
[c] Cemes, CNRS UPR 8011 et Université de Toulouse, 29 rue Jeanne Marvig, 31055 Toulouse, France

ARTICLE INFO

Article history:
Received 26 March 2015
Received in revised form
29 September 2015
Accepted 21 October 2015
Available online 11 November 2015

Keywords:
Spark-plasma-sintering
Electrical and thermal contact
Papyex
Finite element method

ABSTRACT

Spark plasma sintering (SPS) is a breakthrough process for powder consolidation assisted by pulsed current and uniaxial pressure. In order to model the temperature variations of the tools during a SPS cycle, the Graphite-Papyex-Graphite contact phenomena are studied experimentally and modeled by finite element calculations. Compared to conducting materials, the thermo graphic image of an insulating sample (alumina) shows strongly localized heating along the Papyex implying contact effects are predominant. The aim of this modeling study is to determine the main contact phenomena due to Papyex. It is based on numerous experimental data and studies the case of alumina sintering. Finally the contact model is confronted to experimental thermal images.

1. Introduction

Spark plasma sintering (SPS) is essentially a powder consolidation process assisted by pulsed current and uniaxial pressure. It allows sintering of refractory materials in few minutes instead of days by free sintering [1]. The main goal of the thermal modeling of the process is to determine the temperature distribution in the tools and the sample, to experimentally explain any microstructural variations observed, and in the long term to minimize them [2–4]. The SPS column (tools + spacers) detailed in Fig. 1 is usually composed of graphite, to ensure good electrical contact and suitable friction between the inner sliding parts of the tools, a flexible graphite sheet (Papyex® from Mersen) is introduced at the top and bottom of the SPS column and around the sample. The number of papers published on the simulation of the SPS process has drastically increased since the 2000's as has the development of Finite Element Modeling (FEM) software. The first simulations were only devoted to the electro-thermal behavior of the tool (i.e., not the entire column), with or without the presence of the Papyex but not considering its impact on the temperature distribution [5–7]. These simulations allow us to understand the general distribution of the current and the temperature gradient. With the work of Matsugi et al. in 2003 [8,9] SPS modeling started to show a better correlation between the calculated and experimental temperatures.

From 2003 until today SPS modeling has made a lot of progress. The models now include more parts of the SPS column and more physics as for example in the work of Olevsky et al. where the chamber of the SPS and the densification of the sample are modeled simultaneously [10,11]. But in most of these works, the contact resistances generated by the presence of the carbon sheet are not considered.

However, few authors have already made in-situ measurements of the electrical contacts resistance (ECR) in the SPS [12,13], others authors determine the ECR by calibration [14,15]. But using their values, in our model, it is difficult to obtain good experimental accordance because the properties of the contact change with pressure and temperature [16].

In this study we used inverse analysis to identify the contact phenomena at all interfaces of the tool using the temperature distribution revealed experimentally by thermal imaging [17] and/or using thermocouples located at different points of the tool. This work is based on several modeling studies performed at the CIRIMAT and CEMES laboratories on the same configuration of the SPS column [2–4].

* Corresponding author at: CIRIMAT, 118 route de Narbonne, 31062 Toulouse, France. Fax: +33 561556163.
E-mail address: estournes@chimie.ups-tlse.fr (C. Estournès).

http://dx.doi.org/10.1016/j.jeurceramsoc.2015.10.033
0955-2219/

2. Materials and methods

A first set of SPS experiments has been performed using an open die (i.e., a slice was removed) to reveal the internal temperature distribution and to highlight the predominant effects of the electric and thermal contacts for both insulating and conductive samples. Others experiments were made using full die to perform temperature measurements at several points to understand and calibrate the main contact resistances responsible of the high thermal effects revealed by the open die experiments.

2.1. Thermal images on open dies

All the SPS experiments were made on a Dr. Sinter 2080, SPS Syntex Inc., Japan, SPS machine at the "Plateforme Nationale CNRS de Frittage Flash" located at University Toulouse III-Paul Sabatier. The thermal images reported in Fig. 1 were acquired with an infrared camera (FLIR SYSTEMS SC6000) [17]. In this configuration, open molds were used to experimentally measure the internal temperature distribution around the sample. Graphite foils (Papyex) were placed at both interfaces punch/sample and to cover the inner wall of the die (Fig. 2). Fig. 1 shows at low temperature two different cases where pellets of insulating and conducting materials, respectively alumina and copper, were loaded into the die. All the experiments were made on fully dense samples to avoid having to model sintering in the following part.

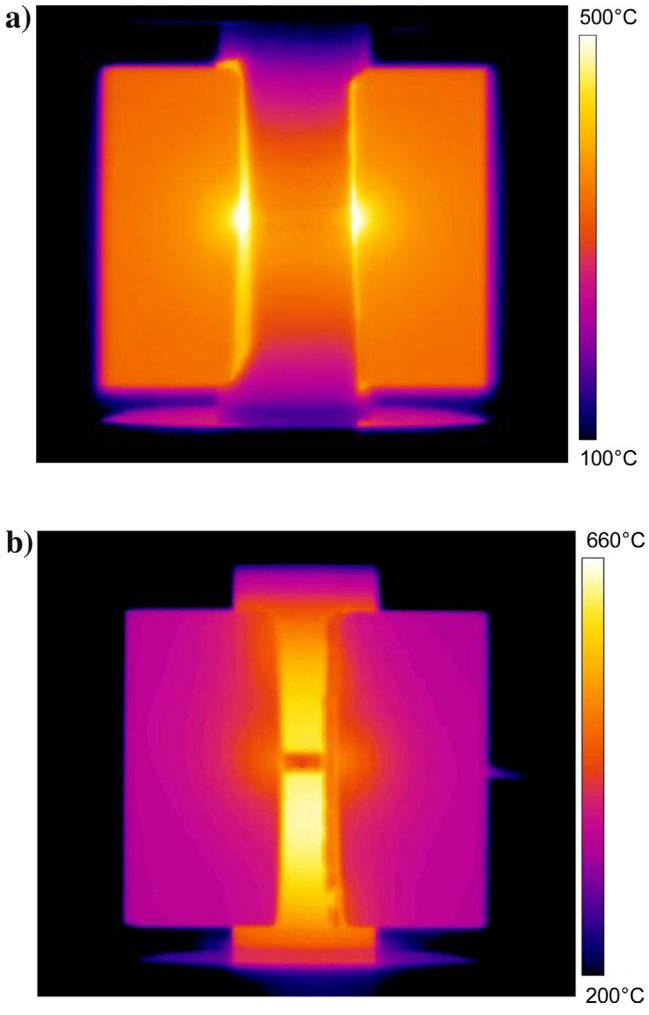

Fig. 1. Infrared thermal images of open die containing: (a) Alumina sample (b) Copper sample.

2.2. Temperature measurements for ECR and TCR calibrations

A double Papyex is classically introduced at both extremities of the SPS column (interfaces spacer/electrode Fig. 2) to ensure a good electrical contact between the inconel electrodes and the graphite spacers. A first experiment was performed with only a graphite part (20 ± 0.05 mm in diameter and 20.55 ± 0.05 mm height) placed between the spacers to calibrate first this spacer/electrode contact resistance. A control thermocouple was located in the graphite part at a depth of 3 mm (Fig. 2a). A second thermocouple was placed on the upper spacer to calibrate the external thermal contact due the double Papyex foils present between the spacer and the inconel (Fig. 2a). High applied pressure (100 MPa) was used to avoid any additional contact phenomena between the graphite part and the spacers.

To calibrate the electrical and thermal contacts around the sample, an experiment similar to that used to obtain the thermal images was performed in a closed mold (Fig. 2b). Two thermocouples were introduced (Fig. 3), one in the die at a depth of 3 mm from its external surface to monitor the SPS temperature and the second inside the die in contact with the graphite foil to calibrate the contact phenomena linked to the use the Papyex sheet. To measure RMS values of pulsed currents a Rogowski coil sensor is used [17].

The calibration of the different ECR and TCR at the interfaces underlined in the two configurations reported in Fig. 2, were performed step by step using an electro-thermal model developed on a finite element code (COMSOL) that will be described in the following section.

3. Theory/calculation: electro-thermal model

The Joule heating model is built up with two main concepts, the current distribution is determined by partial differential Eq. (1).

$$\nabla \times \vec{J} = \nabla \times \left(\sigma \vec{E}\right) = \nabla \times (-\sigma \nabla U) = 0 \quad (1)$$

Secondly the temperature distribution is determined by the heat Eq. (2).

$$\nabla \times (-\lambda \nabla T) + \rho Cp \frac{\partial T}{\partial t} = JE \quad (2)$$

where J is the current density, E the electric field, U the electric potential and for each materials of the device (Fig. 2), σ the electric conductivity, λ the thermal conductivity, ρ the density, Cp the calorific capacity and T the absolute temperature.

There are two main thermal limit conditions:

(i) A radiative flux on the vertical wall of spacers, die, punches and electrodes governed by Eq. (3).

$$\varphi_r = \sigma_s \times \epsilon \times \left(T_e^4 - T_a^4\right) \quad (3)$$

where σ_s is the Stefan–Boltzmann's constant, φ_r the radiative heat flux, T_e the emission surface temperature, T_a the chamber wall temperature, ϵ the emissivity (0.8 for the graphite and 0.67 for the inconel [3]).

(ii) A conducto-convective flux on the horizontal wall of the inconel near the water cooling system (see Fig. 2) is considered and governed by Eq. (4).

$$\varphi_c = h_c \times (T_i - T_w) \quad (4)$$

where φ_c the conducto-convective heat flux, T_i the wall surface inconel temperature, T_w the water temperature, h_c the conducto-convective coefficient (880 $W\,m^{-2}\,K^{-1}$ at the level of the inconel [2]).

The properties of the materials considered are given in Tables A1 and A2.

The Electric Contact Resistance (ECR) and Thermal Contact Resistance (TCR) were, as a first approximation, introduced in the